Predictive multi-scale computational environment for studying epithelial dynamics

Ali Nematbakhsh[1,†], Wenzhao Sun[1,†], Pavel A. Brodskiy[2,†], Cody Narciso[2], Zhiliang Xu[1], Jeremiah J. Zartman[2,*], Mark S. Alber[1, 3, *]

[1] Department of Applied and Computational Mathematics and Statistics, University of Notre Dame, Notre Dame, IN 46556, USA

[2] Department of Chemical and Biomolecular Engineering, University of Notre Dame, Notre Dame, IN 46556, USA

[3] Department of Medicine, Indiana University School of Medicine, Indianapolis, IN 46202, USA

[*]Corresponding authors: malber@nd.edu (M.S. Alber) and jzartman@nd.edu (J.J. Zartman)

[†]These authors contributed equally to the work

Keywords: cellular rearrangements; parallelized subcellular element model; multi-scale, *Drosophila* wing disc; Graphic Processing Units; T1 transition

Abstract

Multicellular development depends in large part on the growth, patterning and morphogenesis of epithelial sheets. How individual epithelial cells coordinate tissue-scale processes is still poorly understood due to the inherent complexity of emergent systems-level behavior. Testing hypothetical novel biophysical mechanisms across spatial scales requires computational models that can span subcellular to tissue levels. However, the task of including detailed descriptions of interactions between the cytoplasm, cortically enriched cytoskeleton and intercellular adhesion is challenging due to the prohibitively high computational costs. Here, we introduce a multi-scale modeling environment called Epi-Scale for simulating epithelial tissue dynamics based on the Subcellular Element (SCE) modeling approach. Epi-Scale explicitly simulates the separate mechanical contributions of multiple cellular components. Computational implementation of the model is based on an efficient parallelization algorithm that utilizes clusters of Graphical Processing Units (GPUs) for simulating large numbers of cells within a reasonable computational time. Epi-Scale naturally recapitulates cellular and tissue-scale properties consistent with experimental data. As a demonstration of the predictive power of the model, detailed simulations of increased cell-cell rearrangements as a function of tissue growth rates are described. A particular advantage for the Epi-Scale environment is its extensibility toward investigating complex biological processes of multiple cell types and interactions between cells and extracellular matrix.

1 Introduction

A fundamental question in biology is how cells are able to communicate and regulate cellular processes to give rise to tissue-scale properties, including the final shape, size and mechanical properties of an organ during development. As one of four basic tissue types in the body, epithelial sheets are significant contributors to the shape and function of organs. Epithelia are composed of tightly adherent cells and provide barriers between internal cells of organs and the environment [1–3] (figure 1). Understanding the regulation of growth in epithelia is also of basic relevance to obtaining a better understanding of the fundamental basis of cancer initiation and progression as 90% of all human tumors are derived from epithelia [4]. The shape (geometry) and cell-cell connectivity, or topological packing, of cells reflect the underlying physical forces acting both at the cellular and tissue scales, which in turn impacts tissue architecture [5]. Interpretation of cell shape and topology promises to provide a quantitative basis for disease identification based on cell morphology [6,7].

Computational modeling coupled with experimentation has become a powerful tool for studying epithelial morphogenesis and homeostasis [8–12]. Multiple approaches have been utilized, each with its own strengths, limitations and primary applications (reviewed in, among others, [13]). The cellular Potts modeling (CPM) approach has been used to study epithelial cells rearrangements [14] and other aspects of morphogenesis [15]. In CPM model the dynamics of each cell, represented by a cluster of lattice points, is determined by a Monte Carlo algorithm. In particular, CPM was successfully used to study the role of cell adhesivity in cell sorting and rearrangements. At the same time, incorporation of detailed representation of cell shapes and mechanical properties into the CPM is computationally costly. As another model, Brodland and colleagues have employed a finite element model to investigate epithelial cells behavior [16,17]. In such models, each cell is composed of multiple triangular shape elements that possess properties such as adhesivity, viscosity and tension along their boundaries. Vertex based model (VBM) is another approach where cells are defined by the number of vertices representing the meeting points of shared cell-cell bonds (reviewed in, among others, [11]). Vertex displacement is governed by minimizing an energy function representing target cell apical area, cell contractility, and cortical tension. A very abbreviated list of applications of vertex based models include: the analysis of the factors that influence the distributions of cell neighbor numbers and

cell properties in cell populations [18], studying mechanical feedback as a possible size regulation mechanism for tissues [19–21], and the role of cell contractility in determining tissue curvature [22]. Finally, SCE modeling is another computational approach , developed initially by Newman [23] for simulating multi-cellular systems, and later extended by Newman and colleagues [24] for studying epithelial cells. In this model each cell consists of a set of nodes representing coarse-grained approximations of subcellular components with node-node interactions determined by energy functions. The main advantage of the SCE approach is the ability to provide detailed representation of mechanical properties of individual cells. The SCE model has been used to predict how cellular mechanical properties and activity give rise to tissue-level properties [25]. The SCE model has also been applied to the study of tissue rheology [26], tissue fusion [27], thrombus formation [28,29], and cell signaling [30].

Despite a considerable variety of approaches, existing epithelial models generally make the assumption that the apical surfaces of cells are polygonal, which is reasonable in some cases but an imprecise approximation in general. For example, this assumption does not hold during mitotic rounding [31–33] which occurs during cell division. Modeling cell rearrangements, known to be important in cell morphogenesis, are typically handled through an *ad hoc* rule that forces cell connectivity changes when a cell bond length falls below a threshold. Furthermore, there is currently no high-resolution, element-based model that completely distinguishes the membrane and actomyosin cortex from the cytoplasm of epithelial cells, yet these are known to have very different mechanical properties [34,35].

Here we describe and calibrate a novel multi-scale modeling environment called Epi-Scale, based on SCE modeling approach, for simulating dynamics and mechanical properties of epithelial tissues. Moving beyond the earlier very important one-component SCE study [24], the key feature of Epi-Scale is that the mechanics of the actomyosin cortex and cytoplasm as well as individual cell membranes are introduced separately as different types of elements in the computational model. An efficient parallelized algorithm that utilizes clusters of GPUs was developed to considerably decrease the computational runtime. Epi-Scale was calibrated using values based on experimental observations of model epithelial systems, in particular relying on literature-based data on the *Drosophila* wing imaginal disc pouch [10,36,37]. Simulation results

show that the Epi-Scale model is capable of reproducing experimentally observed polygon class and cell size distribution of epithelia. The model also predicts a monotonic increase of cell size for cells located in the domain from the center to the edge of epithelial tissues due to the mechanical interactions between cells under growth. Furthermore, the developed model predicts that cell growth rates determine the number of cell rearrangement events. As an extensible platform, the additional subcellular detail provided by the Epi-Scale model enables more realistic dynamical descriptions of epithelial cells, including mitotic rounding, and enables new studies into the underlying biophysical principles of organ development.

This paper is organized as follows. In section 2, we develop and calibrate Epi-Scale for simulating the biophysical interactions of individual epithelial cells at cellular and tissue scales. The platform is implemented in Compute Unified Device Architecture (CUDA) to take advantage of the computational efficiency of GPUs. In section 3, predictive properties of the Epi-Scale are demonstrated by providing quantitative predictions of the distributions of cell areas and cell neighbor statistics in the developing *Drosophila* wing disc. Also potential applications and extensions of the developed model are described. In section 4, we summarize results and provide conclusions.

2 Model development and calibration

2.1 General features

In the Epi-Scale model, individual cells are represented as a collections of subcellular nodes, each with a potential field that describes viscoelastic mechanics [23,24,26,28–30,38]. Each cell is represented by two classes of subcellular nodes: membrane nodes (membrane + actomyosin cortex) and internal nodes (figure 2a). The membrane nodes represent both the plasma membrane and associated contractile actomyosin cortex that provides the membrane's structure [34,35,39,40]. Internal nodes are used as a coarse-grain representation of cytoplasmic contents and resulting bulk mechanical properties within the cell. Membrane and internal nodes are coupled through Morse potentials (figure 2b and figure S.3) [23,30].

Cadherin molecules — such as E-Cadherin — are critical for regulating apical cell-cell adhesion in epithelia [41–44] and are important for organizing adherens junctions (AJ). Adapter proteins connect E-cadherin molecules to cortical actin [45,46], and contribute to epithelial integrity through homotypic binding of cadherin molecules between adjacent cells [43,47–49]. In the model, adhesive interactions between membrane elements on opposing cells are represented as a spring force (figure 2b). This spring-like force provides a coarse grain description of adhesion through homophilic E-cadherin interactions. It only operates when two opposing membrane nodes belong to neighboring cells. Membrane nodes of a cell are connected by a chain of linear and rotational springs forming a closed loop and are used to represent the lipid bilayer of the epithelial cell membrane and associated actomyosin cortex, critical for maintaining the structural integrity of the cell (figure 2c).

Cell growth is simulated by introducing new internal nodes (figure 2d). Internal nodes rearrange through Morse potential interactions (figure 2e). Cell division (mitosis) is modeled by increasing the Morse potential between internal nodes, followed by a division of the cell into two daughter cells with new membrane elements between daughter cells (figure 2f). Specific details about cell growth and division are included in SI.1.2.

2.2 Equations of motion

A typical simulation in the developed model is initialized with seven cells consisting of evenly distributed membrane nodes along an outer ring and randomized seeding of internal elements (figure 3a). After initialization, cellular components freely rearrange to an equilibrium state. Cell-cell adhesion drives the system to form a polygon network as the simulation evolves (figure 3b) through integration of equations of motion described in the following paragraph. The epithelial sheet increases in size due to cell growth and division. The final stage of a simulation is shown in figure 4c when the epithelial sheet reaches 2500 cells. The distribution of cell shapes and sizes in the epithelial cell sheet, shown in figure 4d, is dependent on the balance of mechanical interaction between the cells.

The equations of motion for Epi-Scale model are written by noticing that cell velocities are so small that the inertial term can be ignored in comparison with damping term (overdamped

regime [18,23,50]). Therefore, the membrane and internal nodes equations of motion are written in the following form [51,52]:

$$\eta \dot{\boldsymbol{x}}_{M_i} = -\left(\sum_j \nabla E_{ij}^{MI} + \sum_k \nabla E_{ik}^{MMS} + \sum_l \nabla E_{il}^{MMD} + \nabla E_i^{adh}\right) \quad (2.1)$$

$$\eta \dot{\boldsymbol{x}}_{I_i} = -\left(\sum_j \nabla E_{ij}^{MI} + \sum_k \nabla E_{ik}^{II}\right) \quad (2.2)$$

where η is damping coefficient, $\boldsymbol{x}_{I_i}$ is a position of an internal node, and $\boldsymbol{x}_{M_i}$ is a position of a membrane node. E_{ij}^{MI} is the potential energy function representing mechanical interactions between membrane and internal nodes of the same cell. E_{ik}^{MMS} is the potential energy function describing mechanical interaction between membrane nodes of the same cell. E_{il}^{MMD} represents interaction between two membrane nodes of different cells, E_{ik}^{II} is the potential energy function for describing interactions between internal nodes of the same cell, and finally E_i^{adh} represents adhesion between two membrane nodes of the adjacent cells.

The potential energy functions between different nodes in the computational model are defined by either springs or Morse potential function. Linear and rotational springs are used for modeling E_{ik}^{MMS} and E_i^{adh}, while Morse potential functions are used for modeling E_{ij}^{MI}, E_{ik}^{II}, and $E_{\alpha_i}^{MD}$. Morse potential in general contains components describing short-range repulsive force and longer range attractive force [53]. Following expression shows Morse potential function for E_{ij}^{MI}:

$$E_{ij}^{MI} = \left[\mathrm{U}_{MI} \exp\left(-\frac{|\boldsymbol{x}_i - \boldsymbol{x}_j|}{\xi_{MI}}\right) - \mathrm{W}_{MI} \exp\left(-\frac{|\boldsymbol{x}_i - \boldsymbol{x}_j|}{\gamma_{MI}}\right)\right], \quad (2.3)$$

where U_{MI}, W_{MI}, ξ_{MI}, and γ_{MI} are Morse parameters for E_{ij}^{MI} and calibrated during model testing (Table 1 and figure S3). The same expression with different sets of parameters is used for E_{ij}^{MI} and E_{il}^{MMD}.

Equations of motion of the internal and membrane nodes (Equations 2.1 and 2.2) are discretized in time by an explicit method and positions of nodes $\boldsymbol{x}_{I_i}$ and $\boldsymbol{x}_{M_i}$ are incremented at discrete times. For example, discretized form of the equation of motion of internal nodes (Equation 2.1) is as follows:

$$\boldsymbol{x}_{I_i}^{t+\Delta t} = \boldsymbol{x}_{I_i}^{t} + \left(\sum_j \nabla \left(E_{ij}^{II} \right)^t + \sum_k \nabla \left(E_{\alpha_{ik}}^{MI} \right)^t \right) \frac{\Delta t}{\eta}, \qquad (2.4)$$

where Δt is the time step of the simulation. The same discretization is used for the equation of motion of the membrane nodes.

2.3 Model Calibration

Model parameters are calibrated to simulate experimentally observed behavior of the normal and mitotic cells in the *Drosophila* wing disc system (Table 1; figure 4; model details are provided in SI.1.2). Energy functions for normal cells are chosen to ensure that cells are adhesive enough to attach to each other, while avoiding cell overlapping to satisfy physical boundary conditions. The Epi-Scale model recapitulate physical properties of cells and tissue that are difficult or impossible to obtain by using simpler computational approaches. For example, the initial stages of the simulation capture the transition from nonadherent cells to a colony of adherent epithelial cells (figure 3a, 3b). Other epithelial cell models, such as vertex based models, cannot replicate this physical transition because they enforce a defined connectivity in the form of polygonal shapes.

Energy functions of the mitotic cells were calibrated by comparing simulations of the mitotic rounding of cells during division with experimental data. Mitotic rounding occurs when epithelial cells extend the apical surface and become rounder during mitosis partially due to increased stiffness [31,32,34]. Values and trends for the area and roundness in dividing cells were shown to be consistent with the experimental data (figure 4).

The tissue growth rate in the computational model is assumed to decay exponentially as occurs in real tissues. As described in SI.1.2, the growth rate of each individual cell is assigned randomly based on the decaying growth rate. Values of constants were obtained by calibrating model simulations to obtain the final number of cells observed in the experiments on growing *Drosophila* wing disc pouch.

2.4 CUDA implementation

The main advantage of the Epi-Scale model is the ability to simulate a large number of cells comprising tissues while simultaneously considering detailed cellular interactions. In order to considerably reduce simulation times, an efficient computational framework based on two separate essential features are implemented. First, the simulation is performed on clusters of GPUs, which allows the simulations to run on thousands of nodes concurrently. The computational model is implemented using CUDA, a proprietary parallel computing platform for GPUs. A single graphical card provides significantly higher total computing power compared with a single CPU, but at the cost of increased complexity in code development [30]. Second, we derived an efficient searching algorithm for applying intercellular forces. The most time consuming computational step in the Epi-Scale model is searching for adjacent cells with intercellular interactions (E_{il}^{MMD}) . The search algorithm examines all the cells in the computational domain, which is computationally expensive. To optimize the searching algorithm, a discretized rectangular domain is introduced to limit the search for neighbors to only cells located on neighboring grids (SI text, figure S1). This algorithm considerably reduces the computational time compared to an earlier GPU implementation [30] and results in linear increase in computational time with respect to number of cells. This algorithm is also extensible to three dimensions (3D) since only the nearest neighboring grids are needed. SI.1.1 provides more details about the computational implementation.

3 Results and discussion

3.1 Emergence of tissue size and polygon class distribution

For the selected values of basic parameters (Table 1), Epi-Scale simulation output demonstrates a close approximation to several experimentally observed measurements of tissue organization [5,54]. Approximate tissue-level parameters such as number of cells and growth duration are based on the growth of the *Drosophila* wing imaginal disc pouch during larval growth. The *Drosophila* system has long been used to study epithelial mechanics and consequently has a rich literature of values for constraining simulations. Based on cell cycle times, simulation time corresponds to approximately 100 hours of developmental time in which the number of cells increases from 7 to 2500 cells [55] (Video S1). The final stage of the simulation is shown in figure 5a. One attribute of cells is the number of cell neighbors in contact with a cell. For

instance, a cell with six adhering neighbors can be classified as belonging to the class of hexagonal cells. The polygon class distribution of the same simulation is plotted as function of time in figure 5b and shows the approach to steady state distribution after about 50 hours of simulated tissue growth. Figure 5c shows the comparison of average polygon class distributions of computational results with experimental data for multiple biological systems [24] showing that simulations can be tuned to generally reproduces the experimental data. Both computational and experimental results show that hexagonal cells predominate the shape distribution followed by pentagonal and heptagonal cells respectively. The computational results also demonstrates that increasing in the average cells growth rate will shift the cells polygon class distribution toward cells with higher number of neighbors (sides). This polygon class distribution is an emergent property of the computational model and occurs due to mechanical interactions between cells.

To further verify the Epi-scale model, we have examined whether the simulation results satisfy three relationships known to govern cellular packing distributions in growing and dividing epithelial systems [5,54]. The first is known as Euler's law, stating that the average cell neighbor number for a tissue with a large number of cells should equal to six. Averaging cell size in the final stages of current simulated wing disc shows 5.969 ± 0.002, in very good agreement with Euler's law prediction. The second is known as the Lewis law, which states that the area of a cell should increase linearly as the polygon class of the cell increases. In other word, larger cells should have more sides. Figure 5d shows the numerical results of cell sizes distribution as a function of cell sides, which is in very good agreement with the Lewis law. Finally, Aboav-Weaire law states that the average polygon class of each cell's neighbors decrease as the polygon class of that cell increase. This law is also well satisfied by Epi-Scale as shown in figure 5d. By satisfying these laws, the topology of Epi-Scale simulation output resembles multiple features of biological epithelial topology.

3.2 Emergence of tissue-level properties: cell-cell rearrangements

Epithelial cell-cell rearrangements (T1 transitions) occur as epithelial topology rearranges in response to tissue-level or cell-generated forces [2,56]. During this process, the boundary between two neighbors shrinks to form a 4-sided vertex node (figure 6). This property provides a

measure of the fluidity of cells. T1 transitions are extremely critical for many morphogenetic processes such as convergent extension [14]. However little is known regarding how internal mechanical effects of cells growth and division influences cell rearrangements, even in the absence of directed force generation or application. Figures 6a-c show an example of T1 transition occurring in an experimentally observed developing *Drosophila* wing disc pouch. In figure 6a, cell 3 is a neighbor of cell 1. Figure 6b shows the reducing boundary length connecting cells 1 and 3. Finally, the boundary between these two cells disappears (figure 6c). Figure 6d-f shows an example in the computational model where a similar T1 transition occurs with their dynamics matching experimental observations. In the current model, T1 transitions occurs as an emergent property without the need to define an *ad hoc* rule forcing cell neighbor changes [11,16,18] because cell boundaries are individually defined and free to rearrange.

As the growth rate increases, the number of T1 transitions increase which can be possibly due to the increase in the cells motion due to rapid growth of cells (figure 6g). The low standard deviation of simulations confirms the reliability of the computational results. In these scenarios, it is evident that the T1 transition frequency takes a parabolic shape over time due to a positive contribution from initial increases in cell number and a negative contribution from later decay in growth-rate. Therefore, a maximum value is expected when the number of cells is high enough for expecting high chance of cells rearrangements (T1 transitions) and at the same time enough sources of cells motion due to growth and division, are present in the tissue.

To decouple the effect of cell number and growth rate on T1 transition frequency, scenarios were analyzed where growth rate was varied, but cell number was held constant by only considering the 60 cells closest to the center of the domain (Videos S2-S6). These scenarios resulted in the prediction that T1 transition frequency is correlated with growth rate in epithelial systems (figure 6h).

3.3 Emergence of tissue-level properties: cell size distribution

Understanding how mechanical properties of cells evolve with tissue growth is critical in developing models of cell and tissue size regulation [57]. In figure 7a-d, the cell size distribution as a function of distance from center of wing disc is shown for different simulation times. After a

transitory period of epithelial colony formation, an increase of cell size is observed as the distance from center of epithelial tissue is increased. Higher average radial forces on the cells close to the epithelial disc center and lower average radial forces at the surrounding cells can explain this result. The cells at the center of disc have less freedom and hence are under higher compression from neighboring cells. Therefore, the average cell sizes are lower for cells close to the center of wing disc. The same radial size distribution is also observed in the experimental data for the *Drosophila* wing disc pouch [57,58]. This result strongly supports the interpretation that cell-size gradients arise due to the mechanical interaction between cells independent of chemical signaling.

3.4 Extensions and applications

As a highly extensible modeling platform, Epi-Scale can be expanded to include the third spatial dimension, include multiple cell types, and multiple layers of cells for a large number of cells. This model is designed to handle cell growth and cell division and can be applied to description of morphogenesis and tissue growth dynamics for diverse model systems of epithelia. The effects of external loading on epithelial sheets can be investigated by imposing different forces on the boundary cells. A three-dimensional model would be useful for simulation of epithelial folding, delamination, modeling parenchymal and stromal cell layers, and multi-layer epithelia. Previous studies have predicted that cells grow faster when they are under higher tension, and grow slower while compressed [18,19,59]. Morphogens are also known to regulate the growth rate of epithelial cells [36,60]. With future extension of Epi-Scale to incorporate morphogen signaling, different hypotheses for proliferation regulation can be tested at higher levels of spatial resolution. More generally, Epi-Scale can be modified to simulate general cases of multicellular aggregates. We are also currently extending Epi-Scale to simulating interactions of platelets with the fibrin network as well as contraction of platelet aggregates in blood clots.

4 Conclusions

Here we describe the development and validation of Epi-Scale—a multi-scale, subcellular SCE modeling platform that extends previous subcellular element computational approaches to explicitly model simulate multiple cellular components. Epi-Scale is implemented on clusters of GPUs to handle large scale simulations of dynamics of developing and growing tissues. In Epi-

Scale simulations, polygonal cell-shapes arise from mechanical interactions between cells without pre-defined geometric constraints on the individual cells. The computational model is verified by confirming that the model simulations follows known biological packing behaviors. The computational results show agreement with the Euler, Lewis, and Aboav-Weaire laws. Furthermore, other emerging tissue-level simulation properties were analyzed including a radial cell size distribution that is observed in growing tissues. The developed model was also used to study how cell growth and divisions impact the occurrence of cell-cell rearrangements (T1 transition). The model predicts a strong correlation between the cell growth rate and number of T1 transitions. Increasing the cell growth-rate will increases cell motion with respect to each other, hence leads to higher frequencies of T1 transitions in the tissue. In the future, this result could be tested experimentally by investigating epithelial tissue growth, perhaps of cultured epithelial cell colonies, while chemically or mechanically varying growth rates. Epi-Scale provides extensibility and scalability to handle large-scale multi-scale simulations of tissue growth and morphogenesis, with applications for to studying both development and, cancer biology as well as many other applications such as blood clot formation.

Authors' contributions

Conceived and designed Epi-Scale, experiments and computational study: MSA, ZX and JJZ. Developed and calibrated Epi-Scale: AN, WS, ZX, JJZ and MSA. Imaging and experimental data analysis: CN and PAB. Wrote the manuscript: AN, WS, PAB, CN, ZX, JJZ and MSA. Simulations studies and post-processing: PAB, AN, and WS. Algorithm and code development: WS and, AN, ZX and MSA.

Acknowledgements

This work was support was funded in part by National Science Foundation grant CBET-1403887, DMS-1517293 and NIH grant UO1 HL116330. CN was funded in part by a Berry Fellowship through the Notre Dame Advanced Diagnostics & Therapeutics. The authors acknowledge support from the Notre Dame Integrated Imaging Facility.

References

1. Gumbiner, B. 1987 Structure, biochemistry, and assembly of epithelial tight junctions. *Am. J. Physiol. - Cell Physiol.* **253**, C749–C758.

2. Fristrom, D. 1988 The cellular basis of epithelial morphogenesis. A review. *Tissue Cell* **20**, 645–690. (doi:10.1016/0040-8166(88)90015-8)

3. Lecuit, T. & Lenne, P.-F. 2007 Cell surface mechanics and the control of cell shape, tissue patterns and morphogenesis. *Nat. Rev. Mol. Cell Biol.* **8**, 633–644. (doi:10.1038/nrm2222)

4. Miller, S. J., Lavker, R. M. & Sun, T.-T. 2005 Interpreting epithelial cancer biology in the context of stem cells: tumor properties and therapeutic implications. *Biochim. Biophys. Acta* **1756**, 25–52. (doi:10.1016/j.bbcan.2005.07.003)

5. Sanchez-Gutierrez, D., Tozluoglu, M., Barry, J. D., Pascual, A., Mao, Y. & Escudero, L. M. 2015 Fundamental physical cellular constraints drive self-organization of tissues. *EMBO J.* (doi:10.15252/embj.201592374)

6. Sáez, A., Acha, B., Montero-Sánchez, A., Rivas, E., Escudero, L. M. & Serrano, C. 2013 Neuromuscular disease classification system. *J. Biomed. Opt.* **18**, 066017–066017. (doi:10.1117/1.JBO.18.6.066017)

7. Sáez, A., Rivas, E., Montero-Sánchez, A., Paradas, C., Acha, B., Pascual, A., Serrano, C. & Escudero, L. M. 2013 Quantifiable diagnosis of muscular dystrophies and neurogenic atrophies through network analysis. *BMC Med.* **11**, 77.

8. Brodland, G. W. 2004 Computational modeling of cell sorting, tissue engulfment, and related phenomena: A review. *Appl. Mech. Rev.* **57**, 47–76. (doi:10.1115/1.1583758)

9. Umulis, D. M. & Othmer, H. G. 2014 The Role of Mathematical Models in Understanding Pattern Formation in Developmental Biology. *Bull. Math. Biol.* **77**, 817–845. (doi:10.1007/s11538-014-0019-7)

10. Buchmann, A., Alber, M. & Zartman, J. J. 2014 Sizing it up: The mechanical feedback hypothesis of organ growth regulation. *Semin. Cell Dev. Biol.* **35**, 73–81. (doi:10.1016/j.semcdb.2014.06.018)

11. Fletcher, A. G., Osterfield, M., Baker, R. E. & Shvartsman, S. Y. 2014 Vertex Models of Epithelial Morphogenesis. *Biophys. J.* **106**, 2291–2304. (doi:10.1016/j.bpj.2013.11.4498)

12. Newman, T. J. 2008 Grid-Free Models of Multicellular Systems, with an Application to Large-Scale Vortices Accompanying Primitive Streak Formation. In *Current Topics in Developmental Biology* (ed P. K. M. Stuart A. Newman and Timothy J. Newman Santiago Schnell), pp. 157–182. Academic Press. [cited 2015 Dec. 7].

13. Gibson, W. T. & Gibson, M. C. 2009 Cell topology, geometry, and morphogenesis in proliferating epithelia. *Curr. Top. Dev. Biol.* **89**, 87–114. (doi:10.1016/S0070-2153(09)89004-2)

14. Rauzi, M., Verant, P., Lecuit, T. & Lenne, P.-F. 2008 Nature and anisotropy of cortical forces orienting Drosophila tissue morphogenesis. *Nat. Cell Biol.* **10**, 1401–1410. (doi:10.1038/ncb1798)

15. Chaturvedi, R. et al. 2005 On multiscale approaches to three-dimensional modelling of morphogenesis. *J. R. Soc. Interface* **2**, 237–253. (doi:10.1098/rsif.2005.0033)

16. Chen, H. H. & Brodland, G. W. 2000 Cell-Level Finite Element Studies of Viscous Cells in Planar Aggregates. *J. Biomech. Eng.* **122**, 394–401. (doi:10.1115/1.1286563)

17. Brodland, G. W., Viens, D. & Veldhuis, J. H. 2007 A new cell-based FE model for the mechanics of embryonic epithelia. *Comput. Methods Biomech. Biomed. Engin.* **10**, 121–128.

18. Farhadifar, R., Röper, J.-C., Aigouy, B., Eaton, S. & Jülicher, F. 2007 The Influence of Cell Mechanics, Cell-Cell Interactions, and Proliferation on Epithelial Packing. *Curr. Biol.* **17**, 2095–2104. (doi:10.1016/j.cub.2007.11.049)

19. Aegerter-Wilmsen, T., Heimlicher, M. B., Smith, A. C., Reuille, P. B. de, Smith, R. S., Aegerter, C. M. & Basler, K. 2012 Integrating force-sensing and signaling pathways in a model for the regulation of wing imaginal disc size. *Development* **139**, 3221–3231. (doi:10.1242/dev.082800)

20. Aegerter-Wilmsen, T., Smith, A. C., Christen, A. J., Aegerter, C. M., Hafen, E. & Basler, K. 2010 Exploring the effects of mechanical feedback on epithelial topology. *Development* **137**, 499–506. (doi:10.1242/dev.041731)

21. Hufnagel, L., Teleman, A. A., Rouault, H., Cohen, S. M. & Shraiman, B. I. 2007 On the mechanism of wing size determination in fly development. *Proc. Natl. Acad. Sci.* **104**, 3835–3840. (doi:10.1073/pnas.0607134104)

22. Okuda, S., Inoue, Y., Eiraku, M., Sasai, Y. & Adachi, T. 2013 Apical contractility in growing epithelium supports robust maintenance of smooth curvatures against cell-division-induced mechanical disturbance. *J. Biomech.* **46**, 1705–1713. (doi:10.1016/j.jbiomech.2013.03.035)

23. Newman, T. J. 2005 Modeling multi-cellular systems using sub-cellular elements. *ArXivq-Bio0504028*

24. Sandersius, S. A., Chuai, M., Weijer, C. J. & Newman, T. J. 2011 Correlating Cell Behavior with Tissue Topology in Embryonic Epithelia. *PLoS ONE* **6**, e18081. (doi:10.1371/journal.pone.0018081)

25. Sandersius, S. A., Weijer, C. J. & Newman, T. J. 2011 Emergent cell and tissue dynamics from subcellular modeling of active biomechanical processes. *Phys. Biol.* **8**, 045007. (doi:10.1088/1478-3975/8/4/045007)

26. Sandersius, S. A. & Newman, T. J. 2008 Modeling cell rheology with the Subcellular Element Model. *Phys. Biol.* **5**, 015002. (doi:10.1088/1478-3975/5/1/015002)

27. Flenner, E., Marga, F., Neagu, A., Kosztin, I. & Forgacs, G. 2008 Relating Biophysical Properties Across Scales. In *Current Topics in Developmental Biology* (ed P. K. M. Stuart A. Newman and Timothy J. Newman Santiago Schnell), pp. 461–483. Academic Press. [cited 2015 Dec. 9].

28. Sweet, C. R., Chatterjee, S., Xu, Z., Bisordi, K., Rosen, E. D. & Alber, M. 2011 Modelling platelet–blood flow interaction using the subcellular element Langevin method. *J. R. Soc. Interface* **8**, 1760–1771. (doi:10.1098/rsif.2011.0180)

29. Wu, Z., Xu, Z., Kim, O. & Alber, M. 2014 Three-dimensional multi-scale model of deformable platelets adhesion to vessel wall in blood flow. *Philos. Trans. R. Soc. Lond. Math. Phys. Eng. Sci.* **372**, 20130380. (doi:10.1098/rsta.2013.0380)

30. Christley, S., Lee, B., Dai, X. & Nie, Q. 2010 Integrative multicellular biological modeling: a case study of 3D epidermal development using GPU algorithms. *BMC Syst. Biol.* **4**, 107.

31. Strangeways, T. S. P. 1922 Observations on the Changes Seen in Living Cells during Growth and Division. *Proc. R. Soc. Lond. Ser. B Contain. Pap. Biol. Character* **94**, 137–141.

32. Sanger, D. J. W. 1980 Surface and shape changes during cell division. *Cell Tissue Res.* **209**, 177–186. (doi:10.1007/BF00237624)

33. Cramer, L. P. & Mitchison, T. J. 1997 Investigation of the mechanism of retraction of the cell margin and rearward flow of nodules during mitotic cell rounding. *Mol. Biol. Cell* **8**, 109–119. (doi:10.1091/mbc.8.1.109)

34. Stewart, M. P., Helenius, J., Toyoda, Y., Ramanathan, S. P., Muller, D. J. & Hyman, A. A. 2011 Hydrostatic pressure and the actomyosin cortex drive mitotic cell rounding. *Nature* **469**, 226–230. (doi:10.1038/nature09642)

35. Tinevez, J.-Y., Schulze, U., Salbreux, G., Roensch, J., Joanny, J.-F. & Paluch, E. 2009 Role of cortical tension in bleb growth. *Proc. Natl. Acad. Sci.* **106**, 18581–18586. (doi:10.1073/pnas.0903353106)

36. Restrepo, S., Zartman, J. J. & Basler, K. 2014 Coordination of Patterning and Growth by the Morphogen DPP. *Curr. Biol.* **24**, R245–R255. (doi:10.1016/j.cub.2014.01.055)

37. Neto-Silva, R. M., Wells, B. S. & Johnston, L. A. 2009 Mechanisms of growth and homeostasis in the Drosophila wing. *Annu. Rev. Cell Dev. Biol.* **25**, 197–220. (doi:10.1146/annurev.cellbio.24.110707.175242)

38. Sandersius, S. A., Weijer, C. J. & Newman, T. J. 2011 Emergent cell and tissue dynamics from subcellular modeling of active biomechanical processes. *Phys. Biol.* **8**, 045007.

39. Clark, A. G. & Paluch, E. 2011 Mechanics and Regulation of Cell Shape During the Cell Cycle. In *Cell Cycle in Development* (ed J. Z. Kubiak), pp. 31–73. Springer Berlin Heidelberg. [cited 2015 Dec. 2].

40. Kunda, P., Pelling, A. E., Liu, T. & Baum, B. 2008 Moesin Controls Cortical Rigidity, Cell Rounding, and Spindle Morphogenesis during Mitosis. *Curr. Biol.* **18**, 91–101. (doi:10.1016/j.cub.2007.12.051)

41. Halbleib, J. M. & Nelson, W. J. 2006 Cadherins in development: cell adhesion, sorting, and tissue morphogenesis. *Genes Dev.* **20**, 3199–3214. (doi:10.1101/gad.1486806)

42. Takeichi, M. 1990 Cadherins: A Molecular Family Important in Selective Cell-Cell Adhesion. *Annu. Rev. Biochem.* **59**, 237–252. (doi:10.1146/annurev.bi.59.070190.001321)

43. Roy, F. van & Berx, G. 2008 The cell-cell adhesion molecule E-cadherin. *Cell. Mol. Life Sci.* **65**, 3756–3788. (doi:10.1007/s00018-008-8281-1)

44. Zartman, J. J., Kanodia, J. S., Yakoby, N., Schafer, X., Watson, C., Schlichting, K., Dahmann, C. & Shvartsman, S. Y. 2009 Expression patterns of cadherin genes in Drosophila oogenesis. *Gene Expr. Patterns GEP* **9**, 31–36. (doi:10.1016/j.gep.2008.09.001)

45. Peifer, M., McCrea, P. D., Green, K. J., Wieschaus, E. & Gumbiner, B. M. 1992 The vertebrate adhesive junction proteins beta-catenin and plakoglobin and the Drosophila segment polarity gene armadillo form a multigene family with similar properties. *J. Cell Biol.* **118**, 681–691. (doi:10.1083/jcb.118.3.681)

46. Kobielak, A. & Fuchs, E. 2004 α-catenin: at the junction of intercellular adhesion and actin dynamics. *Nat. Rev. Mol. Cell Biol.* **5**, 614–625. (doi:10.1038/nrm1433)

47. Takeichi, M., Nakagawa, S., Aono, S., Usui, T. & Uemura, T. 2000 Patterning of cell assemblies regulated by adhesion receptors of the cadherin superfamily. *Philos. Trans. R. Soc. Lond. B Biol. Sci.* **355**, 885–890. (doi:10.1098/rstb.2000.0624)

48. Nagafuchi, A. 2001 Molecular architecture of adherens junctions. *Curr. Opin. Cell Biol.* **13**, 600–603. (doi:10.1016/S0955-0674(00)00257-X)

49. Dejana, E. 1996 Endothelial adherens junctions: implications in the control of vascular permeability and angiogenesis. *J. Clin. Invest.* **98**, 1949–1953.

50. Kursawe, J., Brodskiy, P. A., Zartman, J. J., Baker, R. E. & Fletcher, A. G. 2015 Capabilities and Limitations of Tissue Size Control through Passive Mechanical Forces. *PLoS Comput Biol* **11**, e1004679. (doi:10.1371/journal.pcbi.1004679)

51. Kampen, N. G. V. 1992 *Stochastic Processes in Physics and Chemistry*. Elsevier.

52. Newman, T. J. & Grima, R. 2004 Many-body theory of chemotactic cell-cell interactions. *Phys. Rev. E* **70**, 051916. (doi:10.1103/PhysRevE.70.051916)

53. Newman, T. J. 2007 Modeling Multicellular Structures Using the Subcellular Element Model. In *Single-Cell-Based Models in Biology and Medicine* (eds D. A. R. A. Anderson P. M. A. J. Chaplain & D. K. A. Rejniak), pp. 221–239. Birkhäuser Basel. [cited 2015 Aug. 12].

54. Chiu, S. N. 1995 Aboav-Weaire's and Lewis' laws—A review. *Mater. Charact.* **34**, 149–165. (doi:10.1016/1044-5803(94)00081-U)

55. Narciso, C., Wu, Q., Brodskiy, P., Garston, G., Baker, R., Fletcher, A. & Zartman, J. 2015 Patterning of wound-induced intercellular Ca 2+ flashes in a developing epithelium. *Phys. Biol.* **12**, 056005. (doi:10.1088/1478-3975/12/5/056005)

56. Heller, D., Hoppe, A., Restrepo, S., Gatti, L., Tournier, A. L., Tapon, N., Basler, K. & Mao, Y. 2016 EpiTools: An Open-Source Image Analysis Toolkit for Quantifying Epithelial Growth Dynamics. *Dev. Cell* **36**, 103–116. (doi:10.1016/j.devcel.2015.12.012)

57. Mao, Y., Tournier, A. L., Hoppe, A., Kester, L., Thompson, B. J. & Tapon, N. 2013 Differential proliferation rates generate patterns of mechanical tension that orient tissue growth. *EMBO J.* **32**, 2790–2803. (doi:10.1038/emboj.2013.197)

58. LeGoff, L., Rouault, H. & Lecuit, T. 2013 A global pattern of mechanical stress polarizes cell divisions and cell shape in the growing Drosophila wing disc. *Development* **140**, 4051–4059. (doi:10.1242/dev.090878)

59. Aegerter-Wilmsen, T., Aegerter, C. M., Hafen, E. & Basler, K. 2007 Model for the regulation of size in the wing imaginal disc of Drosophila. *Mech. Dev.* **124**, 318–326. (doi:10.1016/j.mod.2006.12.005)

60. Wartlick, O., Mumcu, P., Jülicher, F. & Gonzalez-Gaitan, M. 2011 Understanding morphogenetic growth control — lessons from flies. *Nat. Rev. Mol. Cell Biol.* **12**, 594–604. (doi:10.1038/nrm3169)

FIGURES

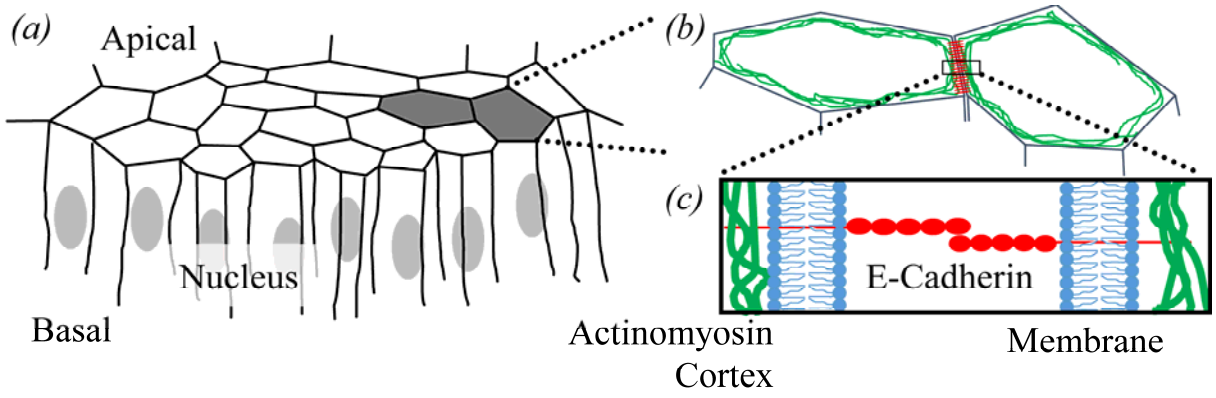

Figure 1. *(a)* Epithelial cells are polarized with apical and basal sides. (b) Apical surface of epithelial cells, which are simulated in Epi-Scale model. *(c)* At the molecular scale, the boundary between cells consists of a lipid bilayer membrane for each cell, E-cadherin molecules that bind to each other through homophilic interactions, and adaptor proteins that connect the adhesion complexes to an underlying actomyosin cortex that provides tensile forces along the rim of apical areas of cells.

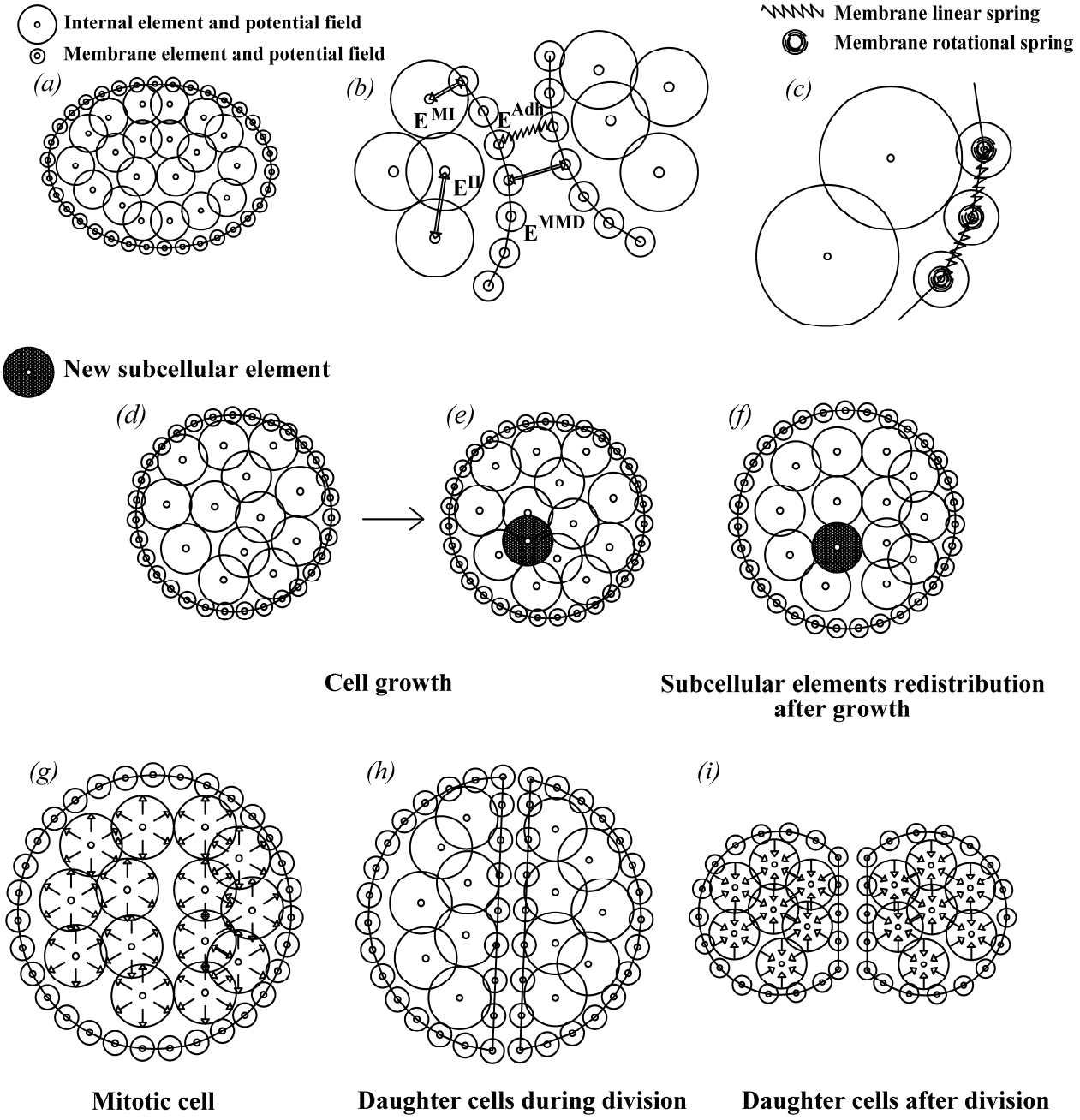

Figure 2. Physics and cell logics in Epi-Scale. *(a)* An illustration of a cell in Epi-Scale model and the relative potential field around each node. *(b)* Intracellular and intercellular interactions between different elements of Epi-scale model. *(C)* Linear and rotational springs are used for modeling cell membrane. *(d-f)* Cell growth in Epi-Scale model: *(d)* initial cell condition, *(e)* cell growth through introduction of new internal nodes, *(f)* rearrangement of cellular nodes after node introduction to balance the energy potential forces. *(g-h)* cell division in the Epi-Scale model: *(g)*

mitotic cells are modeled by changing the Morse parameters for internal nodes interactions, *(h)* division of the elements and creation of a new cell boundary between daughter cells, *(i)* rearrangement of internal nodes after division and return to interphase potential fields.

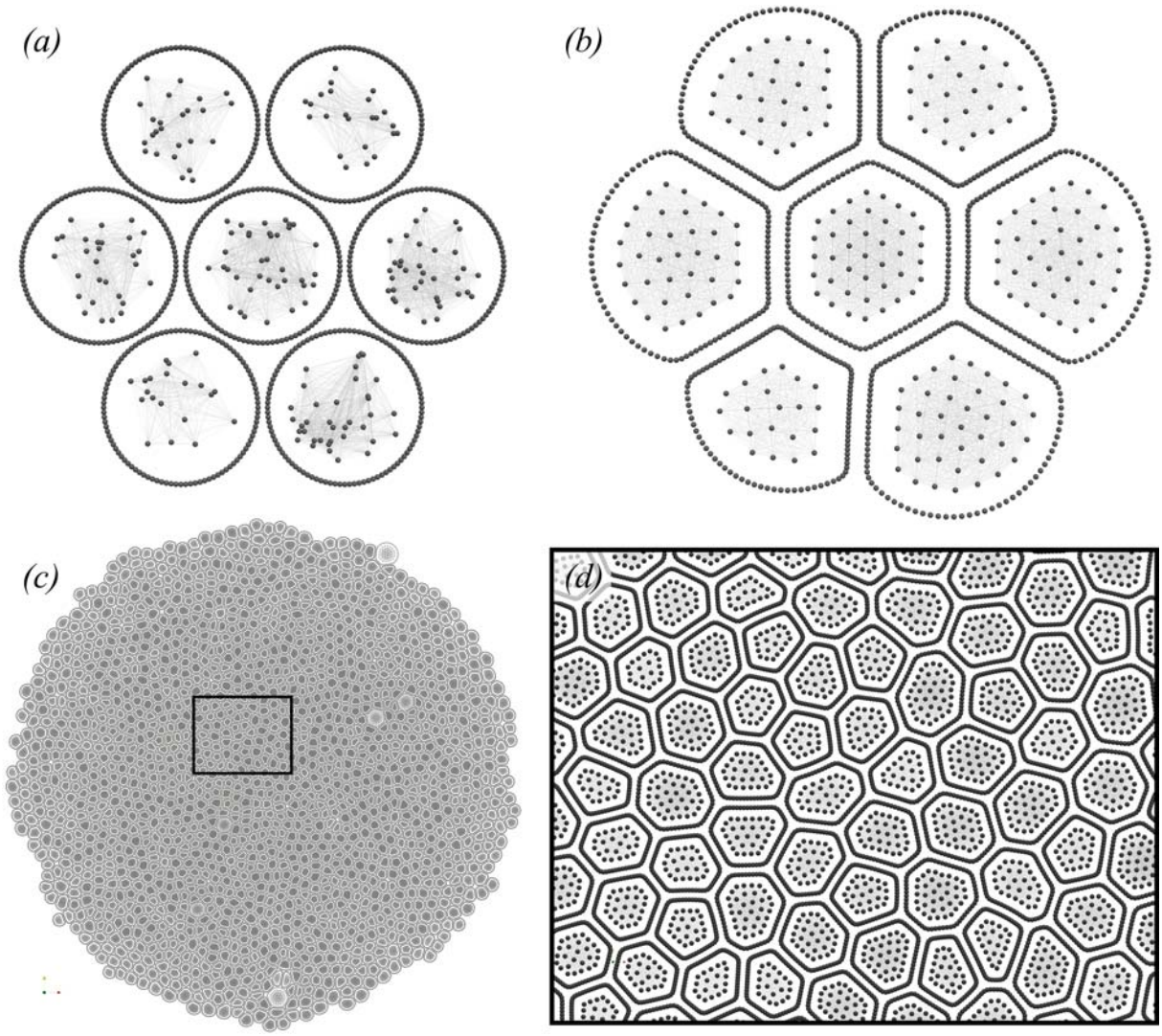

Figure 3. Initial conditions and example simulation. (*a*) Initial condition of an Epi-Scale simulation with seven circular cells. Each cell starts with 100 membrane elements and 20 internal elements. (*b*) Epithelial sheet after cells adhere to each other. An equilibrium distribution of internal nodes is reached for each cell. (*c*) Epithelial sheet near the conclusion of the simulation. (*d*) Enlarged view of the selected region showing different cell shapes and sizes due to mechanical interaction between cells.

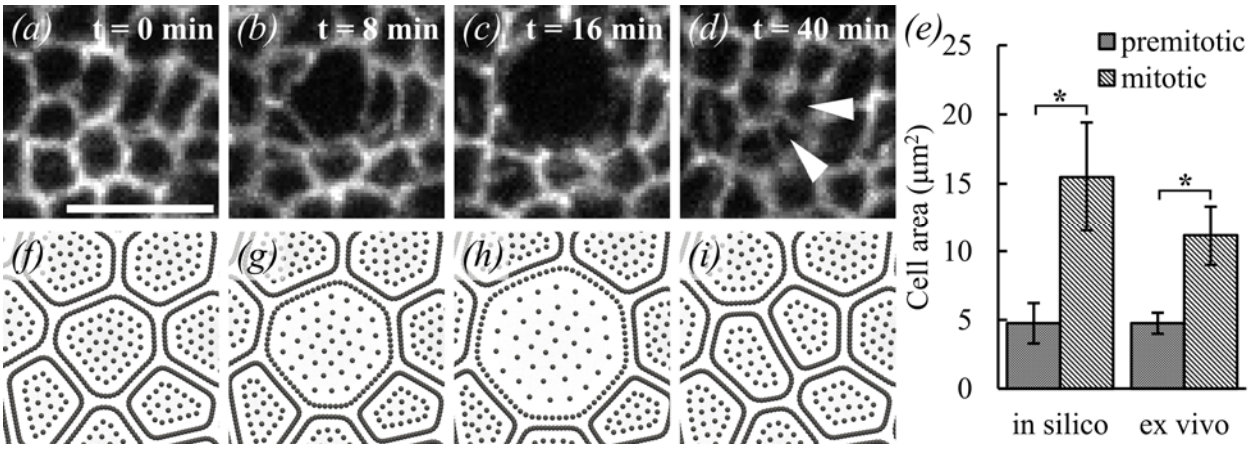

Figure 4. Mitotic rounding calibration. (*a-d*) Mitotic properties were calibrated to experimental data from *Drosophila* wing discs. Time-lapse confocal images of cell undergoing mitosis in the wing disc with E-Cadherin labeling cell boundaries. Scale bar is 5 μm. Arrows indicate daughter cells. (*e*) Area for tracked cells before and during mitosis in *Drosophila* wing disc (*ex vivo*) and Epi-Scale simulation (*in silico*). *(f-i)* Time series from Epi-Scale simulation of a cell undergoing mitosis. * represents $p < 0.05$ by t-test, n = 1754 cells for *in silico*, 24 cells for *ex vivo*. All error bars represent standard deviations.

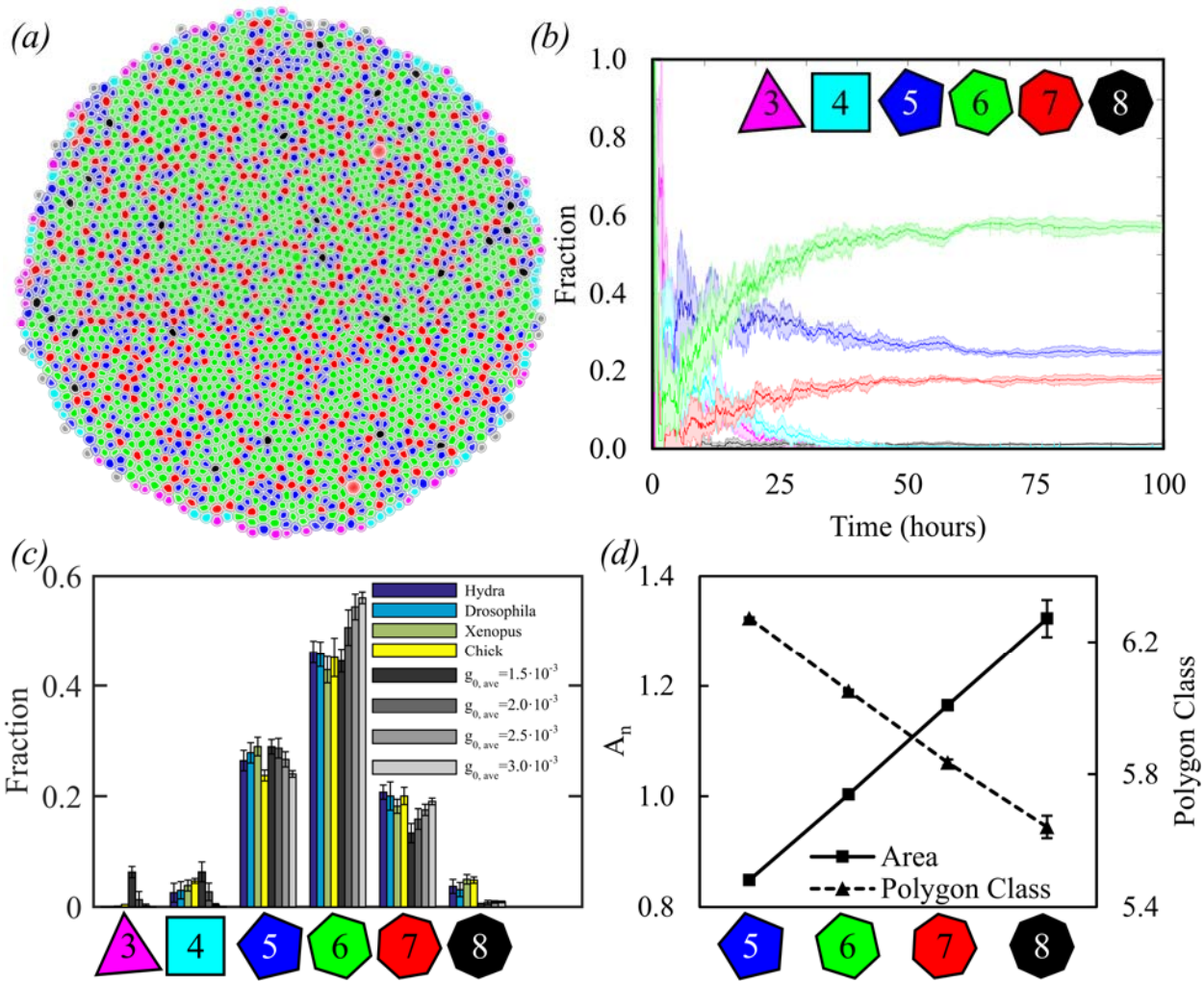

Figure 5. Polygon class distribution (*a*) Sample simulation output showing cells with different numbers of neighbors as different colors. (*b*) Epi-Scale reaches steady-state polygon-class distribution after approximately 50 simulated hours. (*c*) Comparison of polygon class distributions obtained by Epi-Scale model with various biological systems (data extracted from **[24]**). (*d*) Average relative area (A_n) and average polygon class of neighbors for cells of different polygon classes verifying that Epi-Scale simulation results follow Lewis law and Aboav-Weaire law **[54].** Error bars represent standard deviation.

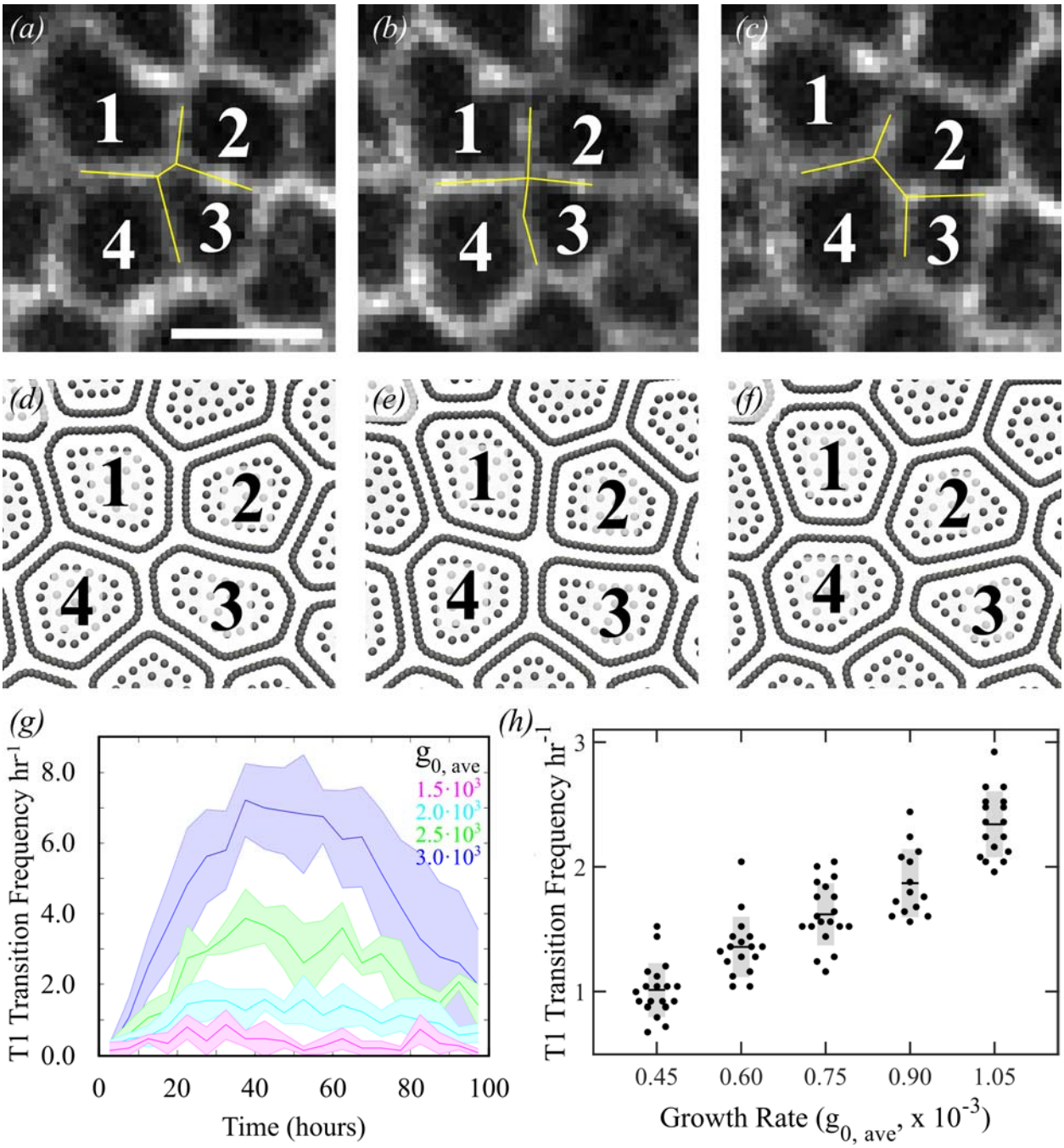

Figure 6. Cell-cell rearrangements (T1 transition) in epithelial cells. (*a-c*) Timelapse confocal images of cells undergoing a T1 transition in the *Drosophila* wing disc, with E-Cadherin labeling cell boundaries, scale bar represents 5 μm. (*d-f*): Time series from Epi-Scale simulation of cells undergoing T1 transition. (*g*) Computational results for average frequency of T1 transitions over simulated time in the whole epithelial disc. (*h*) T1 transition frequency within an unchanging

circular region of interest for computational simulations with varying levels of constant cell growth rate. All error bars represent standard deviations.

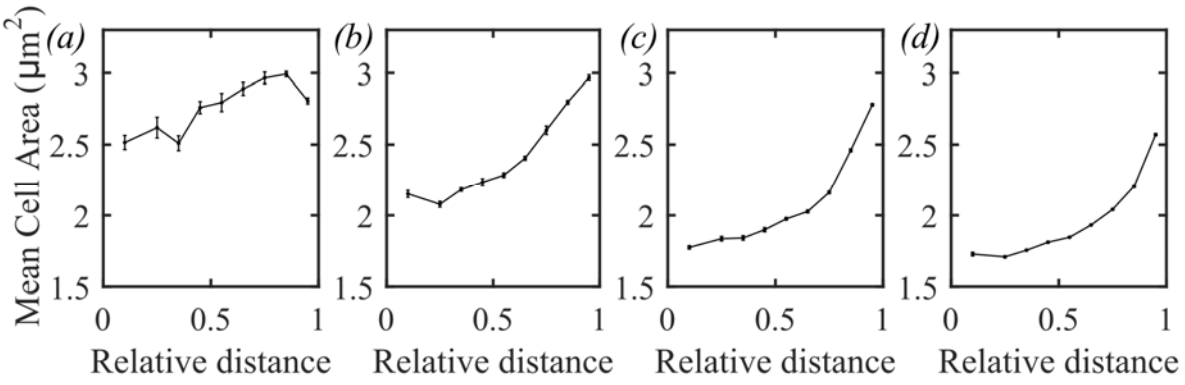

Figure 7. Spatiotemporal gradient of cell sizes. Spatial distribution of cell areas at different time-points (*a*-*d*: 0, 25, 50, 100 hours) and relative positions. In the horizontal axis, 0 represents the center, and 1 is the boundary of simulated epithelial tissue (n=seven simulations). Error bars are s.d. .

Tables

Table 1: Model parameters

Parameter description	Symbol	Interphase cell (Mitotic cell)
Morse parameters for internal-internal interactions (describes contractility)	U_{II}	0.05 (1.5)
	W_{II}	0.015 (0.6)
	ξ_{II}	0.1 (0.15)
	γ_{II}	0.4
Morse parameters for internal-membrane interactions	U_{MI}	0.08 (0.3)
	ξ_{MI}	0.04 (0.07)
Morse parameters for membrane repulsion	U_{MMD}	0.4
	ξ_{MMD}	0.04
Spring parameters for membrane adhesion between different cells	k_{adh}	1.25
	L_{adh}	0.2
Spring parameters for membrane (describes membrane elasticity)	k_{mem}	50
	L_{mem}	0.02
Damping coefficient	η	1
Min. and max of initial growth-rate	$g_{0_{min}}$ & $g_{0_{max}}$	2×10^{-3} & 4×10^{-3}
Growth decay constant	k_g	4×10^{-4}
Mitotic rounding critical value	P_{crit}	0.92

Notes: * Values of variables not written for mitotic cells are kept constant.

** Morse parameters not written are equal to zero.